AD_____

Award Number: W81XWH-11-1-0166

TITLE: Mechanism-Based Enhanced Delivery of Drug-Loaded Targeted Nanoparticles for Breast Cancer Therapy

PRINCIPAL INVESTIGATOR: Hamid Band, M.D.

CONTRACTING ORGANIZATION: University of Nebraska Medical Center
Omaha, NE 68198-6810

REPORT DATE: February 2014

TYPE OF REPORT: Final

PREPARED FOR: U.S. Army Medical Research and Materiel Command
Fort Detrick, Maryland 21702-5012

REPORT DOCUMENTATION PAGE

Form Approved
OMB No. 0704-0188

1. REPORT DATE	2. REPORT TYPE	3. DATES COVERED
February 2014	Final	18 January 2011- 17 January 2014

4. TITLE AND SUBTITLE
Mechanism-Based Enhanced Delivery of Drug-Loaded Targeted Nanoparticles for Breast Cancer Therapy"

5a. CONTRACT NUMBER

5b. GRANT NUMBER
W81XWH-11-1-0166

5c. PROGRAM ELEMENT NUMBER

6. AUTHOR(S)
Hamid Band, MD, PhD; Tatiana Bronich, PhD

E-Mail: Hband@unmc.edu; sraja@unmc.edu; tbronich@unmc.edu

5d. PROJECT NUMBER

5e. TASK NUMBER

5f. WORK UNIT NUMBER

7. PERFORMING ORGANIZATION NAME(S) AND ADDRESS(ES)
University of Nebraska Medical Center
Omaha, NE 68198-6810

8. PERFORMING ORGANIZATION REPORT NUMBER

9. SPONSORING / MONITORING AGENCY NAME(S) AND ADDRESS(ES)
U.S. Army Medical Research and Materiel Command
Fort Detrick, Maryland 21702-5012

10. SPONSOR/MONITOR'S ACRONYM(S)

11. SPONSOR/MONITOR'S REPORT NUMBER(S)

12. DISTRIBUTION / AVAILABILITY STATEMENT
Approved for Public Release; Distribution Unlimited

13. SUPPLEMENTARY NOTES

14. ABSTRACT

The endocytic trafficking pathway is the site of action for receptor-targeted drug-delivery strategies, including Antibody-Drug-Conjugates (ADCs) and nanoparticle drug-delivery systems. Effective drug-release requires trafficking of the endocytosed receptor-bound cargo into the lysosomes for efficient disintegration. However, cancer-cell specific alterations that lead to receptor recycling, instead of lysosomal-degradation, can dampen the efficiency of drug delivery. Such changes include receptor overexpression, increased association with the molecular chaperone, chaperones such as HSP90 or alterations in regulators of recycling versus lysosomal pathways (Rab GTPases, c-Src, deubiquitinases). While substantial effort has gone into designing receptor-targeted drug delivery systems, the consequence of factors leading to altered recycling versus lysosomal trafficking on the efficiency of drug delivery have not been considered.

The receptor tyrosine kinases ErbB2 and EGFR, which are often overexpressed in breast cancer, are examples of cell surface receptors used for evaluating nanoparticle-based targeted drug delivery systems. However, several studies have established that the ErbB2 receptor is either endocytosis-impaired or undergoes rapid recycling, suggesting that the strategies to enhance receptor internalization and lysosomal routing could further enhance the efficacy of cytotoxic drug being delivered. While, the molecular chaperone HSP90 is critical for maintaining oncogenic ErbB2-activity, it also is thought to be responsible for the altered trafficking of the receptor. The objective of this synergistic DOD-IDEA grant proposal was to evaluate our innovative hypothesis that HSP90 inhibitors can facilitate ErbB2-targeted delivery of chemotherapeutic payloads.

The studies reported here successfully demonstrate, as we hypothesized, that concurrent administration of a low, non-toxic, dose of HSP90 inhibitor 17AAG substantially enhanced the efficacy of doxorubicin-loaded, Trastuzumab-conjugated nanogels, and led to xenograft tumor regression. These novel findings should pave the way for endocytic mechanism-based enhancement of receptor-targeted drug delivery using nanogels.

15. SUBJECT TERMS- none provided

16. SECURITY CLASSIFICATION OF:			17. LIMITATION OF ABSTRACT	18. NUMBER OF PAGES	19a. NAME OF RESPONSIBLE PERSON
a. REPORT	b. ABSTRACT	c. THIS PAGE			USAMRMC
U	U	U	UU	19	19b. TELEPHONE NUMBER *(include area code)*

Table of Contents:

Introduction:

Breast cancer continues to remain the leading type of cancer among women and second leading cause of cancer-related deaths in the U.S according to the statistics released by the American Cancer Society. In 2013, there were more than 2.8 million breast cancer survivors and over 232,340 new cases of invasive breast cancer were expected to be diagnosed (http://www.breastcancer.org). Nearly a third of breast cancer patients are diagnosed to be positive for the Human Epidermal Growth Factor Receptor 2 (Her2; also known as ErbB2 or Neu) and therefore represent a major therapeutic target. The humanized anti-ErbB2 monoclonal antibody, Trastuzumab (Herceptin, Genentech, San Francisco, CA), is now an essential part of treatment of ErbB2 - overexpressing breast cancers. Trastuzumab is currently administered with other chemotherapeutics, like microtubule stabilizing agents (Docetaxel, Paclitaxel), DNA binding drugs (Doxorubicin, Epirubicin, Cisplatin) or alkylating agents (Cyclophosphamide). However, clinical data indicate a less than satisfactory response rate in patients and importantly, most patients that do respond initially eventually develop resistance. In addition to the tumor cells acquiring resistance, the patients also have to endure the effects of the chemotherapeutics on the normal tissue. Anti-ErbB2 antibody-conjugated polymeric nanoparticles with a capacity to load multiple drugs at high concentrations represent a promising alternative to circumvent these problems. However, success of ErbB2-targeted drug-delivery into the cytosol using nanotechnology platforms critically depends on the efficiency of internalization. Optimal targeting must therefore take into account the biology of endocytic trafficking of ErbB2 receptor (1-3). Specifically, the low rate of endocytosis is attributed to constitutive association of ErbB2 with Heat Shock Protein 90 (HSP90) (2, 3). This Synergistic IDEA project seeks to develop a novel strategy to effectively target ErbB2-overexpressing breast cancer with anti-ErbB2 antibody- coated nanogels carrying potent chemotherapeutics in combination with HSP90 inhibitors to enhance the endocytosis of ErbB2 receptor-bound nanogel cargo. A successful outcome of our studies will provide a new therapeutic approach against a particularly difficult form of breast cancer and may provide a template for therapeutic targeting of other forms of breast cancer and other cancers. Success in preclinical models would also provide strong rationale for clinical translation of this technology with the ultimate goals of selective delivery of imaging and therapeutic modalities to tumors.

Grant Hypothesis/Objective and Specific Aims: In this original grant, we had hypothesized that the efficacy of treatment of ErbB2-overexpressing cancers using targeted delivery of cytotoxic payload encapsulated in nanogels based on copolymer micelles can be vastly improved by simultaneously targeting ErbB2-HSP90 complex using HSP90 inhibitors and optimizing ErbB2 endocytosis. The specific aims for this proposal were:

1) Develop novel nanogels based on copolymer micelles with ionic cross-linked cores carrying anticancer chemotherapeutics (single drugs and combinations) and decorated with an anti-ErbB2 antibody for targeting to ErbB2-overexpressing breast cancer cells;

2) Optimize the intracellular delivery of targeted nanogels carrying cytotoxic drugs to ErbB2-overexpressing breast cancer cells based on HSP90 inhibitor-facilitated internalization of ErbB2;

3) Demonstrate enhanced efficacy of 17-AAG to deliver cytotoxic cargo encapsulated in targeted nanogels using in vivo xenograft mouse models.

Summary: This is an integrated final report describes the efforts devoted by the partnering PI's (Dr. Bronich) research team with the biological studies done by the Initiating PI's (Dr. Hamid Band) research team to meet the major objectives that were set forth in the statement of work.

Synthesis of nanogels: Fabrication of the nanogels involves condensation of diblock copolymers of poly(ethylene oxide) (PEG) and poly(carboxylic acid) by divalent metal cations into spherical micelles of core-shell morphology. The micelle core is cross-linked further through the use of bifunctional agents and cations are removed by dialysis. The resulting hydrophilic nanospheres combine several key structural features: a cross-linked ionic core; a hydrophilic PEG shell; and nanoscale size (Figure 1). A highly hydrated porous ionic core can efficiently entrap various charged therapeutic agents while hydrophilic PEG chains provide increased solubility and prevent interactions of plasma components with the nanosphere. Nanoscale size is essential to avoid renal excretion and to facilitate extravasation of micelles at the tumor site. Each of these nanogels is in essence a single nanostructured copolymer. Therefore, the proposed polymer system is resistant to extremely dilute conditions that occur upon intravenous injection. The multiple end groups in the PEG shell of the nanogel may be readily modified with vector ligands, targeting antibodies for active targeting, leading to multivalent recognition of probe targets. Cross-linked nanogels were prepared by template-assisted method using a two-step process, which includes 1) condensation of block ionomers with Ca^{2+} ions into spherical self-assembled block ionomer complexes (BIC) and 2) cross-linking reaction of BIC templates by bifunctional agents using the procedure described in our previous reports and publications (4-6). Doubly hydrophilic copolymers containing anionic and nonionic hydrophilic polymeric segments (block ionomers) were used for the synthesis of nanogels. Polymethacrylic acid (PMA) and polyglutamic acid (PGA) were used as anionic blocks. Poly(ethylene oxide), PEG, was used as a hydrophilic block. The characteristics of block copolymers used in these studies are summarized in Table 1. Diblock copolymer samples are denoted as PEG(x)-b-PMA(y) or PEG(x)-b-PGA(y), where x and y represent the degree of polymerization of the PEG segment and PMA or PGA segment, respectively.

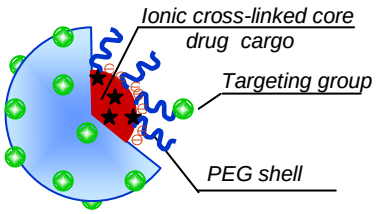

Fig. 1. Schematic representation of targeted polymer micelle with cross-linked ionic core

Table 1. Characteristics of block copolymers

Block copolymer[a]	Molecular weight	Polydispersity index
PEG(170)-*b*-PMA(180)	23,000	1.45
PEG(125)-*b*-PMA(180)	21,000	1.16
PEG(114)-*b*-PGA(100)	20,600	1.22
PEG(114)-*b*-PGA(150)	27,500	1.38

[a]The average number of ethylene oxide and carboxylic acid units (in parentheses) in block copolymers were calculated using the average molecular weights provided by manufacturer

Nanogels were synthesized using the general procedure as was described earlier (6). Briefly, PEG-*b*-PMA/Ca^{2+} complexes were prepared by mixing an aqueous solution of PEG(170)-*b*-PMA(180) with a solution of $CaCl_2$ at a molar ratio of $[Ca2^{+}]$ /$[COO^{-}]$=1.1. The inner core of the micelles formed was cross-linked through the carboxylic groups using bifunctional agent, 1,2-ethylenediamine, in the presence of 1-(3-dimethylaminopropyl)-3-ethylcarbodiimide hydrochloride (EDC) at appropriate molar ratios to achieve the desired theoretical extent of cross-linking. The theoretical extent of cross-linking has been controlled by the ratio of amine functional groups to carboxylic acid groups of block-polymer. It should be noted, that actual extent of cross-linking were expected to be significantly less (4), due to side reaction between water and the activated carboxylic groups. Moreover, it is quite likely that some

portion of the diamine could form a “loop” being bound to the same PMA chain as well as attach by one amino group giving the free amine. It has been estimated that approximately two cross-links per block copolymer chain were formed in the micelles with targeted 20% degree of cross-linking. The reaction mixture was allowed to stir overnight at room temperature. The byproducts of the cross-linking reaction and metal ions were removed by exhaustive dialysis of the reaction mixtures, against (4) 0.5% aqueous ammonia in the presence of ethylenediaminetetraacetic acid (EDTA), and (5) distilled water. The resulting nanogels were of ca. 130 nm in diameter and had a net negative charge (ζ-potential = -22 mV). The core of such micelles comprised a swollen network of the cross-linked PMA chains and was surrounded by the shell of hydrophilic PEG chains. The hydrogel-like behavior of these micelles was observed upon a change of pH. Their size increased considerably with increasing pH, which was completely reversible. The particles were stable and revealed no size change even upon a 100-fold dilution.

We explored the effects of the hydrophobicity and the length of cross-linker on the structure and swelling properties of the cross-linked micelles using several diamino cross-linkers. 1,2-ethylenediamine, 1,5-diaminopentane, cystamine HCl, and 2,2’-(ethylenedioxy)bis (ethylamine) were used to cross-link the cores of template PEG(170)-*b*-PMA(180)/Ca^{2+} micelles with targeted degree of cross-linking from 10% to 60%. The incorporation of more hydrophobic cross-linkers into the core of the micelles resulted in the formation of polymer micelles with smaller sizes. Conventional solution-state ^{1}H NMR allowed us to estimate the changes in the extent of cross-linking upon the synthesis. As expected, the number of cross-links introduced into the core of the micelles increased with the increase of targeted degree of cross-linking. Furthermore, the number of cross-links in the micelles was elevated when more hydrophobic cross-liker was used. As a result the swelling of the core of such micelles upon increase of pH was suppressed: only a modest increase in the D_{eff} was observed for the micelles with hydrophobic cross-linkers (e.g. 1,5-diaminopentane).

Stable biodegradable cross-linked polymer micelles were prepared using PEG-b-poly(glutamic acid) block copolymers (PEG(114)-b-PGA(100) and PEG(114)-b-PGA(150)). In contrast to PEG-b-PMA copolymers, PEG-b-PGA copolymers were able to form block ionomer complexes only in the presence of metal ions of higher valency such as Al^{3+} or Gd^{3+}. The synthesized PEG-b-PGA nanogels were of 100-300 nm in diameter and were readily degradable in the presence of proteases. For example, in the presence of ca. 7 units of protease from Bovine pancreas the PEG-b-PGA nanogels were degraded within 4 hours at 37^{o}C.
To enable solubilization of the relatively hydrophobic drug 17-AAG into the nanogel core, hydrophobic moieties were introduced into the core-forming segments of PEG(114)-b-PGA (150) nanogels. Specifically, PGA block was modified with hydrophobic phenylalanine moieties (Phe) via carbodiimide chemistry using Phe methyl ester (degree of modification was 30% as determined by 1H NMR). Such amphiphilic copolymer, PEG-b-PPGA, readily formed PEG-b-PPGA/Ca^{2+} complexes-templates and allowed to prepare polypeptide-based nanogels of small size (ca. 72 nm at pH 7).

Drug-loaded nanogels: A weakly basic drug doxorubicin, DOX, (pKa = 8.2) was immobilized into the cores of PEG(170)-b-PMA(180) nanogels that contain PMA, a weak polyacid (apparent pKa is 5.5), by simple mixing of this drug with the aqueous dispersion of the nanogels. Nanogels were prepared using relatively hydrophobic cross-linker, 1,5-diaminopentane (DAP). Briefly, the aqueous solutions of DOX (2 mg/ml) and polymer nanogels were mixed at pH 7 and incubated for 24 h at room temperature. The composition of the mixtures expressed as the feeding molar ratio of DOX to carboxylate groups (R=[DOX]/[COO^{-}]) was kept at 0.5. Free unbound DOX was removed thoroughly by repeated filtrations through a 30kDa molecular cutoff membrane pretreated with the drug to retain only the DOX- loaded nanogels. As expected, drug loading was accompanied by a decrease in both the size and net negative charge (ζ-potential) of the nanogels (effective diameter D_{eff}=138.9±4.3 nm, ζ-potential = - 34.0 ±2.6 mV vs. D_{eff}=115.0±1.1 nm, ζ-potential = - 18.1±3.1 mV for initial and DOX-loaded nanogels). This is consistent with the neutralization of the PMA chains upon DOX binding to carboxylate groups, resulting in reduction of the osmotic swelling pressure inside the cores of nanogels. A substantial drug loading level (up to 50% w/w) was achieved and it was strongly

dependent on the structure of the nanogels. For example, maximal loading capacity (expressed as mass of incorporated DOX per mass of DOX-loaded nanogels) of nanogels with DAP cross-links and 60% targeted degree of cross-linking was 55.2%, while nanogels with cystamine cross-links and 20% targeted degree of cross-linking exhibited loading capacity of 42.5%. DOX-loaded nanogels maintained their dispersion stability and exhibited no aggregation or precipitation for a prolonged period of time (up to several months). It is of interest to note that binding of DOX to the PEG-b-PGA nanogels, resulted in the formation of large aggregates with low dispersion stability, perhaps, because the resulting DOX/PGA complex was too hydrophobic and the PEG segments in the corona of the nanogels were unable to stabilize the particles in dispersion. The release profiles were examined for DOX-loaded nanogels with various cross-links in the core to address the effect of the nanogel structure on DOX release. All types of micelles displayed sustained release of DOX under physiological conditions and no burst release was observed. Of particular interest was the finding that the rate at which DOX was released from the nanogels with more hydrophobic cross-links (DAP, cystamine) in the core was substantially slower (Fig. 2).

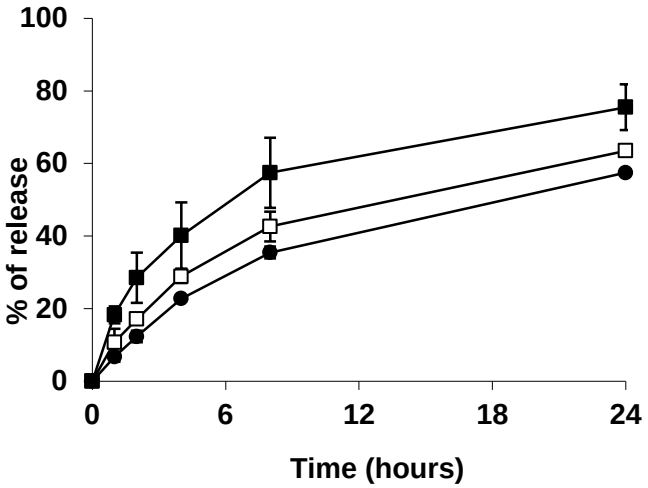

Fig. 2. Release profiles of DOX from PEG-b-PMA nanogels (20% targeted degree of cross-linking) with various cross-links in the cores: ehylenediamine (■); DAP (□); cystamine (●). The loading capacity of DOX for each sample is 200 μg. The data represent averaged values and standard deviations calculated based on three independent experiments.

To solubilize 17-AAG into DOX-loaded nanogels we used the thin-film dissolution method. Appropriate amount of 17-AAG was dissolved in methanol and after complete removal of the solvent, the films dried in vacuo for at least 3 h to remove residual solvent. Subsequently an aqueous solution of empty or DOX-loaded nanogels were added to the vial and incubated for 24 h. Unbound 17-AAG was removed by filtration through HPLC syringe filters (0.45 mm pore size). The concentration of DOX present in the nanogels was quantified spectrophotometrically using the absorbance at 410 nm. The concentration of 17-AAG was determined by HPLC analysis under isocratic conditions using an Agilent 1200 system. As stationary phase an Agilent Eclipse XDB C18-5μm column was used (150 x 4.6 mm), a mobile phase of acetonitrile/10mM ammonium acetate containing 0.1v% acetic acid (pH 4.8) mixture (50/50, v/v) was applied. The co-encapsulated ratios of Dox : 17-AAG were estimated to be 7.8:1 w/w within PEG-b-PMA nanogels whereas it was 1.4:1 w/w for the PPGA nanogels. The physicochemical characteristics of drug-loaded nanogels are presented in Table 2.

Table 2. Physicochemical characteristics of drug-loaded nanogels

Nanogel	Particle size (nm)	PDI	ζ-potential (mV)
PEG-b-PMA	144.5	0.109	-32.8
PEG-b-PMA /DOX	98.6	0.154	-22.1
PEG-b-PMA /DOX+17-AAG	105.9	0.080	-19.7
PPGA	82.5	0.185	-45.5
PPGA /DOX	69.3	0.198	-22.7
PPGA/DOX+17-AAG	57.4	0.161	-21.5

Particle size, polydispersity index (PDI) and ζ-potential were determined by dynamic light scattering at pH 7.0.

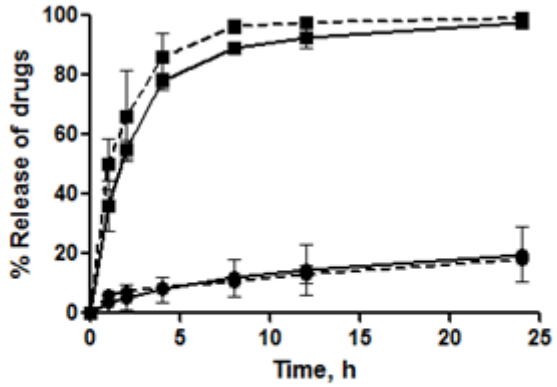

Fig. 3. Drug release profiles for DOX(□) and 17-AAG (■) from combination formulation (solid lines) and single formulation PPGA nanogels (dashed lines) in PBS, pH 7.4.

The release profile of the encapsulated drug from the nanoparticle carrier is crucial for the activity of the drug. Figure 3 shows the cumulative release profiles of DOX and 17-AAG from the PPGA-based nanogels at physiological pH and temperature. As seen from these data sustained but temporally distinct release of DOX and 17-AAG was observed. For example, during 12 hrs (DOX+17-AAG)/NG released ~ 50% of loaded 17-AAG and only ~ 17% of loaded DOX. Notably, 17-AAG release was much faster than that of DOX, which is expected since 17-AAG is physically entrapped into the hydrophobic domains in the PPGA nanogels. In contrast, DOX binds with PGlu chains through electrostatic and van der Waals interactions and its release usually proceeds via ligand exchange reactions with biologically abundant anions, thus delaying its liberation from the nanogels. .

***Cellular uptake of 17-AAG and Dox encapsulated in nanogels is via the endocytosis of the micellar formulations (Initiating and Partnering PI)*:**

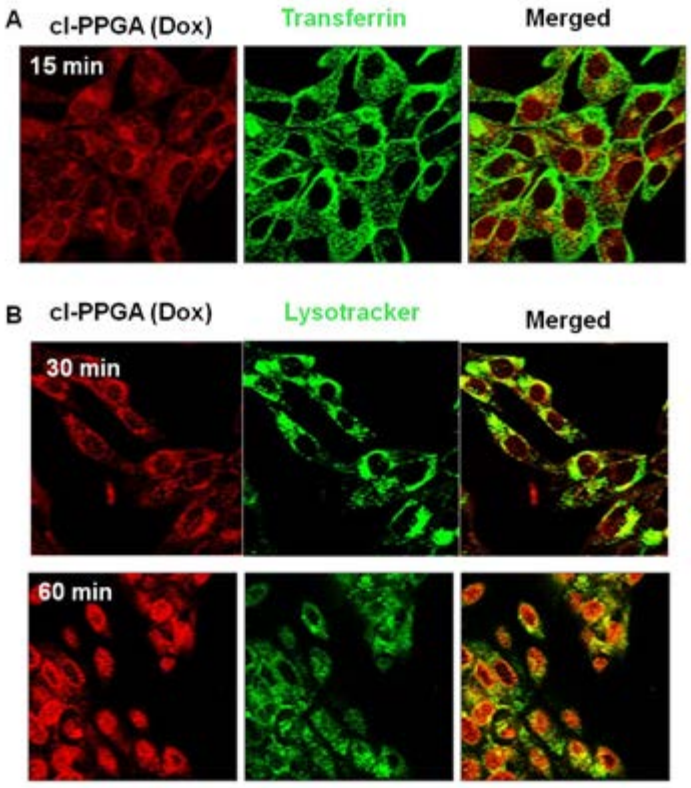

Fig. 4 Confocal Immunofluorescence analysis of distribution of Dox-nanogels within early endosomes (Transferrin-positive) and in lysosomal (Lysotracker positive) compartments in 21MT-1 cell line.

Confocal microscopy tracking the Dox uptake in live cells, confirmed that the Dox-loaded cl-PPGA micelles accumulated in Transferrin positive early endosomes within 15 min (seen as colocalized yellow punctuate structures in Fig. 4A, merged panel) and within 30 was within lysosomes (as seen by colocalization with lysotracker dye in Fig. 4B, merged panel). As seen in the low-resolution microscopy images shown in Fig. 4, most of the fluorescence from Dox was within the cytosol and not the nucleus at 30 min. However by 60 min, the Dox fluorescence was found in the nucleus, confirming diffusion of DOX from the lysosomes, presumably following disintegration under the lysosomal pH, redox conditions and lysosomal proteases, such as Cathepsins.

Previous studies from our lab has shown that BIC nanogels with crosslinked ionic cores can be selectively endocytosed into cancer cells, which lack tight epithelial cell junctions, in contrast to normal epithelial cells that form tight junctions (7). The internalization route appeared to be predominantly via the caveolar pathway. While the current studies report the ability of untargeted BIC nanogels to be internalized into ErbB2-overexpressing breast cancer cells, our goal and ongoing work is aimed at develop anti-ErbB2 antibody-conjugated nanogels encapsulating chemotherapeutics in combination with HSP90 inhibitors to achieve ErbB2-targeted drug delivery specifically into ErbB2 breast cancer cells.

4) *HSP90 inhibitory activity of 17-AAG released from nanogel (Initiating PI)*: While the intrinsic fluorescence of Dox served as a method to follow the uptake of untargeted nanogels and Dox-release, we followed ErbB2 degradation as a means to assess the release of 17-AAG and its ability to inhibit intracellular HSP90. The results are shown in Fig. 5 demonstrates that the encapsulated 17-AAG is released into the cytosol and can inhibit HSP90 leading to ErbB2-degradation. As seen in Fig. 5A, the dose response for ErbB2 degradation induced by cl-POMA and cl-PPGA formulations of 17-AAG were similar to free 17-AAG; similarly the kinetics of ErbB2 degradation were also similar to the free 17-AAG (Fig. 5B).

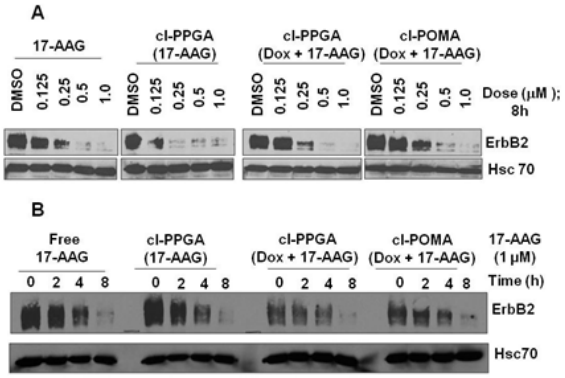

Fig. 5 Nanogel encapsulated 17-AAG can induce ErbB2-degradation in 21MT-1 cell line as efficiently as free 17-AAG. Comparison of dose response (A) of kinetics (B) for ErbB2-degradation induced by 17-AAG nanogels with free 17-AAG. Equal amounts of cell lysates following treatment was loaded on an SDS-PAGE and analyzed by Western blotting. Shown here are changes in ErbB2-levels at the indicated doses (A) or treatment-times (B). Hsc70 is shown as a loading control.

Cytotoxicity of Drug-loaded nanogels against ErbB2-high and ErbB2-low breast cancer cell lines: In the above described studies we optimized the conditions for preparation of Dox plus 17-AAG co-encapsulated nanogels. Following our initial assessment of its cytotoxic activity in 21MT-1 cell line, we extended the study to compare sensitivities (in terms of IC_{50}) for ErbB2-high versus ErbB2-low cell lines. Two additional ErbB2-overexpressing breast cancer cell lines, BT-474 (Trastuzumab-sensitive) and JIMT-1 (Trastuzumab-resistant)(8) and the ErbB2-low expressing breast cancer cell line, MCF-7, was used for these studies. The results are as shown in Table 3. Interestingly, the synergistic interaction between Dox plus 17-AAG was much more apparent (in terms of the reduction in the IC_{50} values for Dox plus 17-AAG as compared to free Dox; for the ErbB2 overexpressing cell lines 21MT-1 and BT-474 (the two Trastuzumab-sensitive cell lines) as well as the Trastuzumab-resistant JIMT-1 cell line than for the ErbB2-low MCF-7 cell line. Indeed, the higher IC_{50} values seen for JIMT-1, relative to 21MT-1 and BT-474 may be because of the lower ErbB2-levels. We also compared the cytotoxicity of two different BIC nanogels (cl-POMA and cl-PPGA) co-encapsulating Dox plus 17-AAG against the cell line panel and confirmed that both formulations retained the synergistic effects of the combination (compare IC_{50} values for free Dox + 17-AAG with cl-POMA or cl-PPGA-Dox-17-AAG) nanogels as shown in the table). Interestingly, while the activities of the two formulations were comparable in the case of 21MT-1 and JIMT-1, the cl-PPGA formulation seemed to have about 6-fold higher activity for BT-474 and MCF-7 as compared to cl-POMA. The reason for relatively higher efficacy of cl-PPGA formulation is presently unclear.

Table 3. Comparison of IC_{50} values for free drug vs. drugs loaded in nanogels against ErbB2 + and ErbB2 – cell lines as determined by the MTT assay.

Dox formulation	IC_{50} (μM) [with respect to Dox]			
	21MT-1	BT-474	JIMT-1	MCF-7
Free Dox alone	0.74	5.5	8.7	3.1
Free Dox + 17-AAG	0.066	0.025	0.77	1.35
cl-POMA (DOX + 17-AAG)	0.32	0.49	4.54	4.57
cl-PPGA (DOX + 17-AAG)	0.46	0.084	2.87	0.79

In vivo DOX release from nanogels: Drug release and biodistribution of DOX-loaded nanogels were evaluated in female nude athymic 4 week old mice bearing ectopic A2780 human ovarian cancer xenograft tumor (300-400 mm^3) after a single i.v. bolus dose (n=5) of free DOX or DOX-loaded nanogels at 6 mg DOX/kg of animal. The pharmacokinetic profiles of DOX and DOX-loaded nanogels in plasma are presented in Fig.6. Free DOX was rapidly cleared from the blood compartment after i.v. injection. In contrast, the DOX-loaded nanogels showed an initial rapid clearance from the blood, followed by slow clearance after 2h post injection. The plasma concentration of DOX incorporated in nanogels was significantly higher than that of free DOX 2h after injection. The PK parameters were evaluated using non-compartmental analysis with WinNonlin software. An estimated terminal elimination half-life was significantly extended from 5.8h for DOX to 36.9h for DOX-loaded nanogels, while the total clearance of DOX delivered by nanogels was estimated to be 1513.9 ± 335.1 mL/kg/h, four fold less than for free DOX (6039.4 ± 1590.1 mL/kg/h). As a result of reduced plasma clearance, DOX formulated in nanogels exhibited prolonged blood circulation. Indeed, the area under the plasma concentration - time curve ($AUC_{0\rightarrow\infty}$) value for DOX-loaded nanogels was four-fold greater than that of free DOX up to 48 h. Nanogels significantly altered tissue distribution of DOX. In particular, tumor accumulation of DOX-loaded nanogels (approximately 1.6 % of injected dose per g tissue) was twice higher than for the free DOX and was maintained at the elevated level for at least 48h. On the other hand, tumor concentrations of DOX were maximal at 5 min post dosing of free DOX and then sharply decreased. $AUC_{0\rightarrow48h}$ for DOX-loaded nanogels in the tumor was 2.7-times greater than that of free DOX (Table 4). These data suggest that DOX was effectively delivered to the tumor by means of polymeric nanogels. Furthermore, the DOX concentrations in the heart, kidneys and lungs were significantly reduced by DOX-loaded nanogels, in contrast to the increasing level of DOX in the tumor. It is well known that DOX levels in the heart and kidneys are related to the cardiac toxicity and nephrotoxicity of DOX (8, 9). The significant reduction in distribution of DOX to heart and kidneys indicates the potential of nanogels in reducing adverse effects associated with DOX therapy. On the other hand, DOX-loaded nanogels were distributed mainly in the organs of the reticuloendothelial system such as the liver and spleen. Such high uptake of nanoparticles in liver and spleen has been reported for other drugs, which are incorporated in polymeric carriers including pegylated liposomes (10, 11).

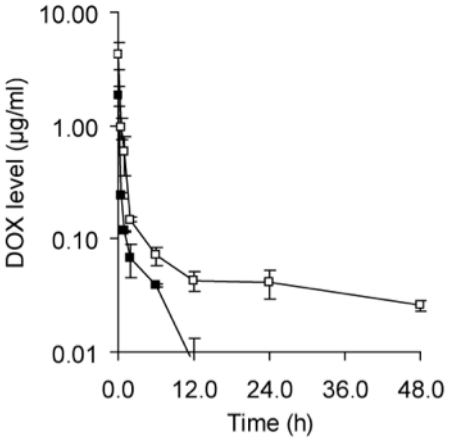

Fig. 6 Pharmacokinetic profiles of free DOX (■) and DOX incorporated into nanogels (○) in the plasma after i.v. injection at a single dose of 6mg/kg. The data represent the mean ± SD (n=5).

Table 4. Biodistribution of DOX and DOX-loaded cl-micelles after injection in A2780 tumor-bearing mice at a single dose of 6mg/kg.

Organ	$AUC_{0\rightarrow48h}$		AUC ratio[a]
	Free DOX	DOX-loaded nanogels	
Tumor	32	86	2.7
Heart	175	63	0.4
Liver	147	425	2.9
Spleen	218	1601	7.3
Kidney	75	69	0.9
Lung	222	90	0.4

[a]AUC ratio = AUC of DOX-loaded nanogels/AUC of free DOX

Synthesis and characterization of anti-ErbB2 antibody (Trastuzumab) modified nanogels:

In our study mAb (Trast and mouse igG) were attached to the nanogels via strepthvidin-biotin complex (Fig. 7). Briefly, streptavidin was attached to the nanogels via PEG cross-linker (Mw 10 kDa) followed by conjugation to biotinylated Trast. The Trast-nanogels were purified by SEC on Sepharose CL-6B. This purification procedure allowed removing all unbound mAb, while the unmodified and mAb-conjugated nanogels were not separated. After coupling the size of the particles slightly increased from 110 nm to ca. 160-170 nm. Practically the same results were obtained for nanogels modified with non-specific mouse IgG. The mAb-conjugated nanogels remained stable in PBS, pH 7.4, exhibiting no aggregation for several weeks. Specific interactions between mAb-modified nanogels and its targeted antigen, ErbB2, on the surface of cancer cells were examined by flow cytometry and confocal microscopy. Flow cytometry analysis revealed strong specific binding of these targeted nanogels to ErbB2-overexpressing breast cancer cells (Fig. 8) comparable to free Trastuzumab antibody. These data suggest that as a result of decoration of the nanogels with the specific antibodies, the Trast-nanogels acquire ability for strong interaction with its targeted antigen.

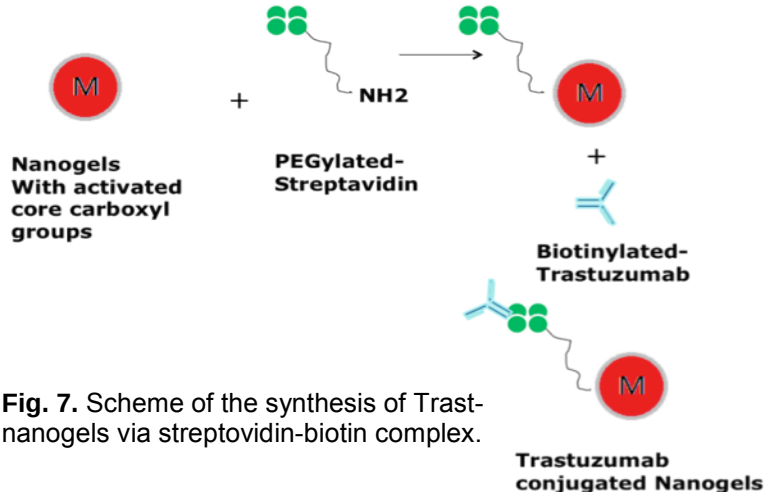

Fig. 7. Scheme of the synthesis of Trast-nanogels via streptovidin-biotin complex.

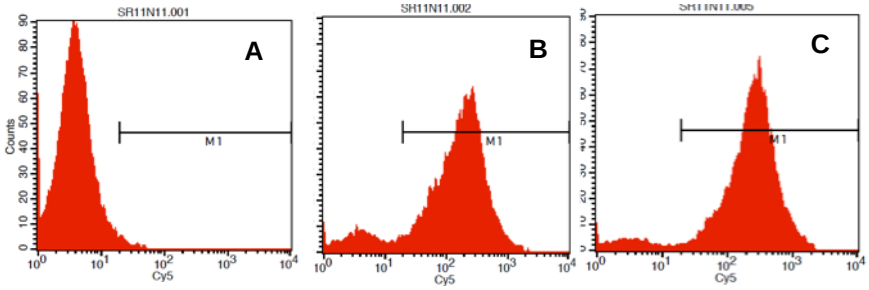

Fig. 8. FACS analysis of binding of Trast-nanogels prepared via streptavidin-biotin complex to ErbB2-overexpressing breast cancer cells. (A) Cy5-labeled secondary Ab alone; (B) biotinylated Trast + Cy5-Sec; (C) Trast- nanogels + Cy5-Sec.

Demonstration that HSP90-inhibition facilitates trafficking of Trastuzumab-nanogels into lysosomal compartments: Confocal Immunofluorescence analysis done on SKBr-3 cells, as presented in Fig. 9 confirmed that the nanogels (green) were found in LAMP-1 (a lysosomal marker, red) positive compartments.

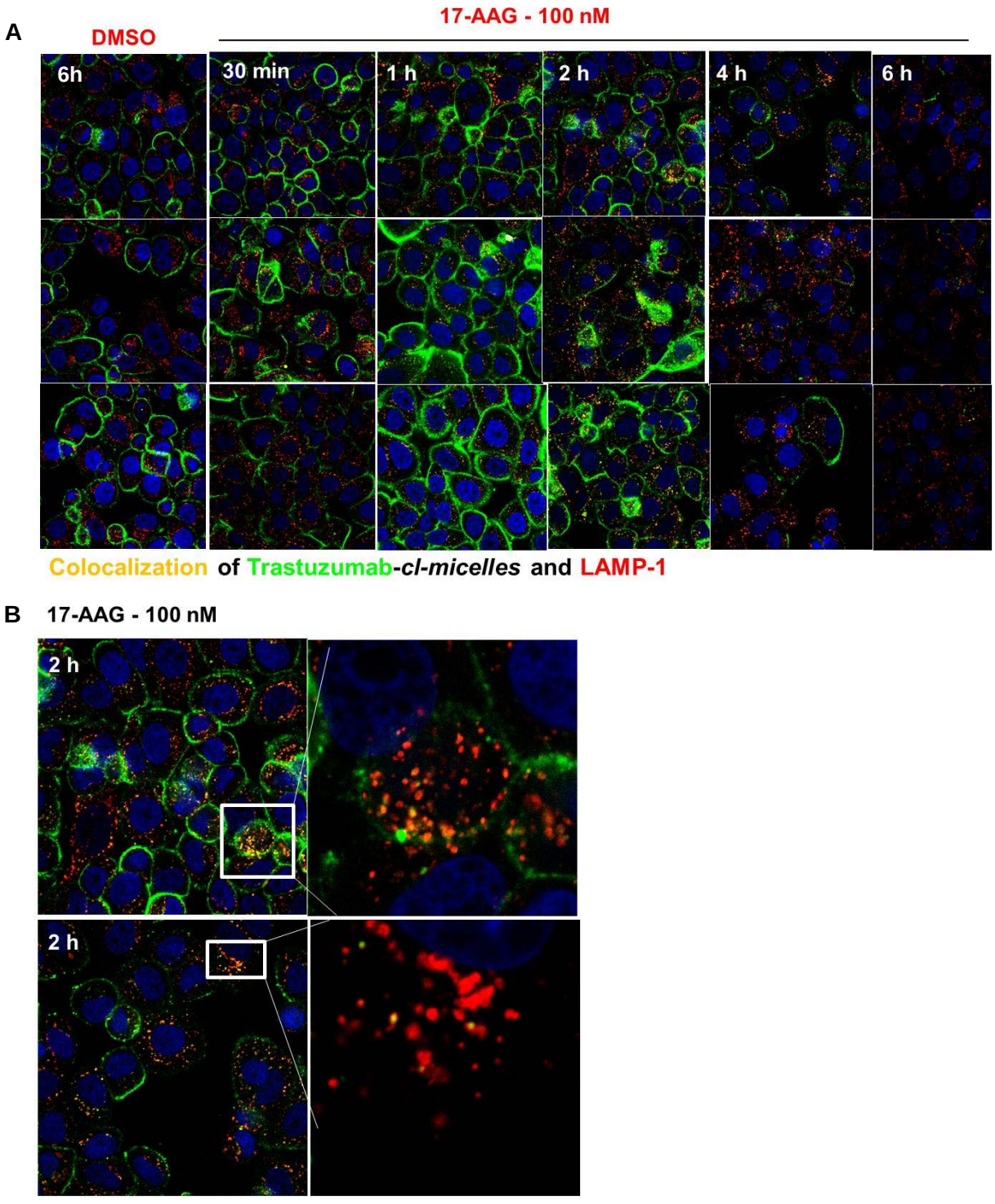

Fig. 9 *A,* Trastuzumab-nanogels (without drugs) was bound to ErbB2-overexpressing SKBr3 cells, plated on glass coverslips, for 1h. 17-AAG (100 nM) was added for the indicated times, after which the slides were washed and fixed in 4% parafolmaldehyde. Nanogels were visualized by staining the Fc-portion of Trastuzumab using FITC-conjugated anti-Human antibody (green), whereas the lysosomal marker LAMP-1 was stained using mouse anti-human LAMP-1 mAb, followed by Alexa-594-conjugated anti-mouse secondary. Shown here are three independent fields analyzed by confocal immunofluorescence microscopy. B, a zoom image of boxed regions from two independent fields demonstrating co-localization (yellow) of the nanogels (green) with LAMP-1 (red).

Demonstration that HSP90-inhibition enhances the cytostatic effect of Doxorubicin delivered via Trastuzumab-nanogels specifically in ErbB2-overexpressing breast cancer cells: Having verified our central hypothesis that HSP90-inhibition facilitates the routing of Trastuzumab-nanogels (without drugs) into the lysosomes, we evaluated the ability of 17-AAG to enhance the delivery of Doxorubicin (a model chemotherapeutic) encapsulated within the nanogels. The ErbB2-overexpressing cell line, 21MT-1 was used for these experiments. Doxorubicin-loaded Trastuzumab-conjugated nanogels (Dox-T-NG; at varying concentrations) were incubated with 21MT-1 cells for 6 hours, following which cells were either left alone (control) or treated with 100 nM 17-AAG for 18 hours to trigger internalization and lysosomal routing of the targeted nanogel cargo. Similar experiments on the ErbB2-low cell line MCF-7 were done in order to confirm ErbB2-specific delivery. Biological effects were assessed by evaluating Doxorubicin-induced G2/M arrest. The results are shown in Fig. 10-12. As expected, there was clear increase in the % of ErbB2-overexpressing 21MT-1cells that underwent G2/M arrest upon 17-AAG-treatment as compared to cells that were not treated with 17-AAG, at varying doses of Dox-T-NG tested (see Fig. 10). On the other hand, no appreciable difference of 17-AAG was noted in similar experiments conducted on the ErbB2-low MCF-7 cells (Fig. 11) especially at lower concentrations of Dox-T-NG.

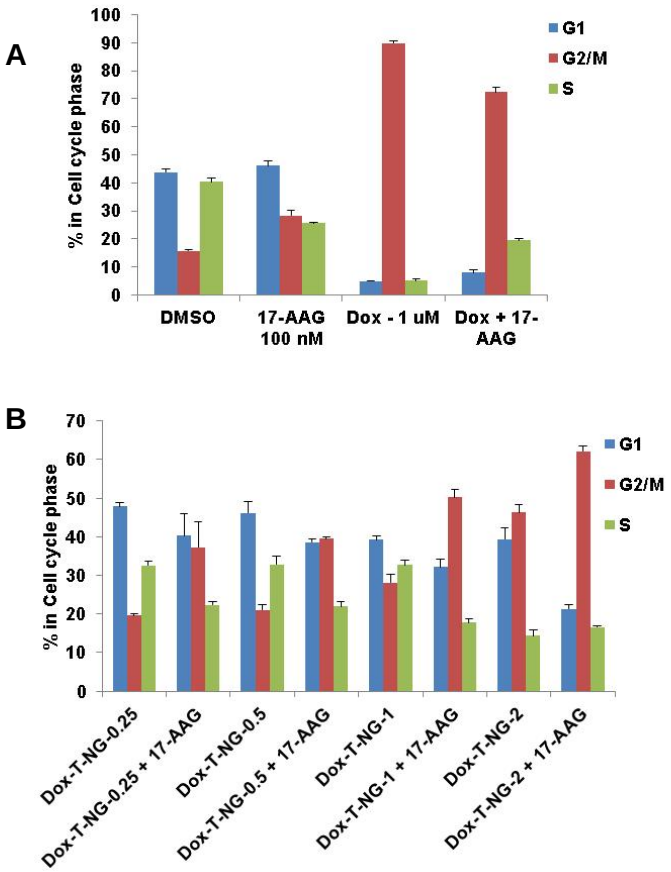

Fig. 10 The ErbB2-overexpressing cell line, 21MT-1, plated in 6-well plates (triplicate wells for each treatment condition) was treated with free Doxorubicin (1 μM) or the indicated concentrations of Dox-T-NG for 6h. The concentrations indicated are with respect to the Trastuzumab conjugated to the NG (in μg/ml). The media was removed and cells were then washed with Phosphate buffered saline (PBS), before replacing with fresh drug-free media alone or media containing 17-AAG (100 nM) for 18 h. The following day, the cells were once again washed and allowed to incubate with drug-free media for an additional 24 h (total 48 hours). After 48 h, the cells were trypsinized, washed twice with PBS and fixed in cold ethanol, for subsequent cell-cycle analysis. The % of cells in various phases of cell cycle for each treatment condition is shown above. Panel *A*, shows the results for free drug treatment, whereas panel *B* depicts the outcome for Dox-T-NG.

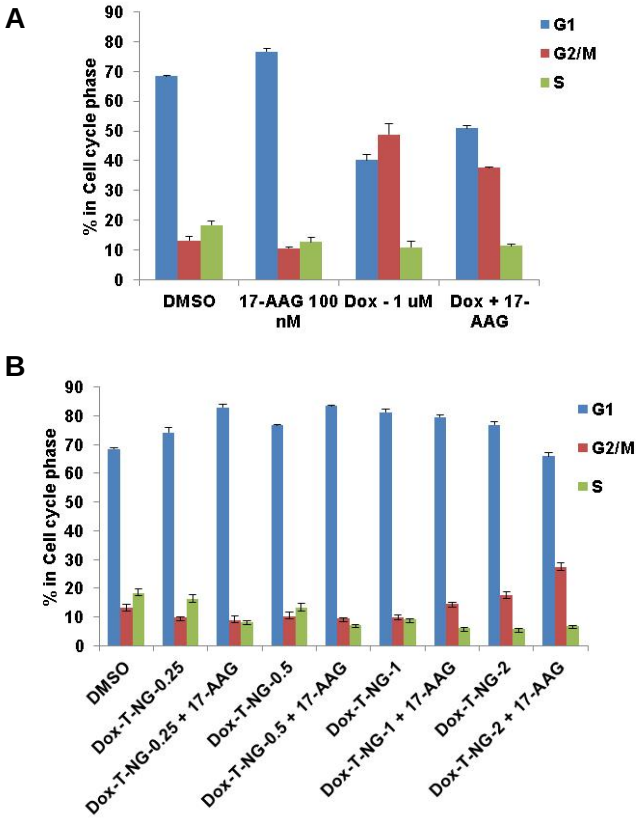

Fig. 11 The ErbB2-low cell line, MCF-7, plated in 6-well plates (triplicate wells for each treatment condition) was treated with free Doxorubicin (1 μM) or the indicated concentrations of Dox-T-NG for 6h. The media was removed and cells were then washed with Phosphate buffered saline (PBS), before replacing with fresh drug-free media alone or media containing 17-AAG (100 nM) for 18 h. The following day, the cells were once again washed and allowed to incubate with drug-free media for an additional 24 h (total 48 hours). After 48 h, the cells were trypsinized, washed twice with PBS and fixed in cold ethanol, for subsequent cell-cycle analysis. The % of cells in various phases of cell cycle for each treatment condition is shown above. Panel *A*, shows the results for free drug treatment, whereas panel *B* depicts the outcome for Dox-T-NG.

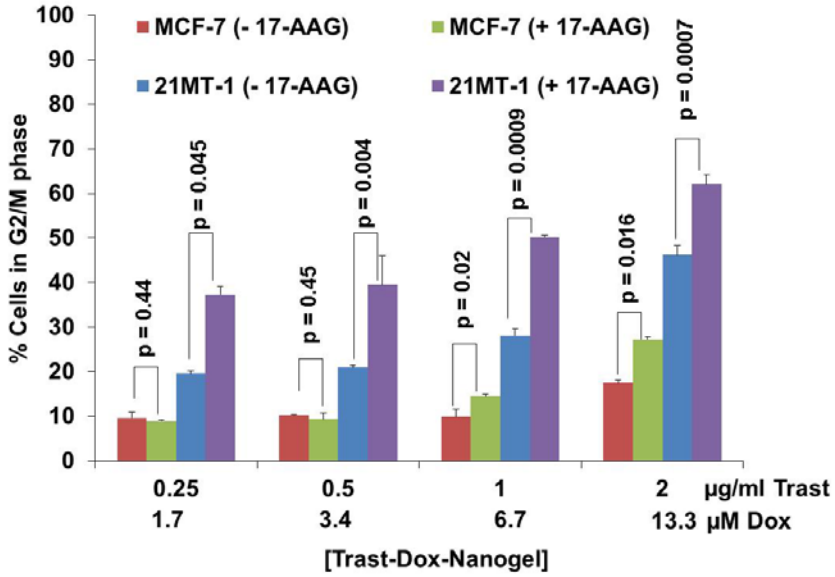

Fig. 12 Shown here is the comparison of the effect of Dox-T-NG, with/without 17-AAG treatment on 21MT-1 and MCF-7 cell line (data from Fig. 10 & 11).

Demonstration that HSP90-inhibition enhances the cytostatic effect of Doxorubicin delivered via Trastuzumab-nanogels specifically in ErbB2 + breast cancer mice models:

Having verified our central hypothesis that HSP90-inhibition facilitates the routing of Trastuzumab-nanogels (without drugs) (Trast-NG) into the lysosomes, we also evaluated the ability of Trast-NG/DOX (without 17 AAG) to enhance the delivery of encapsulated Doxorubicin compared to non-targeted NG/DOX.

Table 5. Comparison of IC_{50} values for targeted Vs non targeted nanogels against ErbB2 + and ErbB2 – cell lines as determined by the MTT assay.

Formulation	IC_{50} (μM)	
	BT-474 (ErbB2 +)	MCF-7 (ErbB2 -)
NG/DOX	0.43 ± 0.13	0.29 ± 0.1
Trast-NG/DOX	0.07 ± 0.08	0.19 ± 0.07

The ErbB2-overexpressing cell line, BT-474, was used for these experiments. Trast-NG/DOX and NG/DOX were incubated with BT-474 cells for 48 hours. Similar experiments on the ErbB2-low cell line MCF-7 were done in order to confirm ErbB2-specific delivery. Biological effects were assessed by MTT assay. The results are shown in Table 5. There was 6-fold reduction in the IC50 value when cells were treated with Trast-NG/DOX compared to NG/DOX in ErBb2-overexpressing cells. On the other hand, no appreciable difference of Trastuzumab conjugation was noted in similar experiments conducted on the ErbB2-low MCF-7 cells.

To further support our hypothesis, we conducted antitumor efficacy of our treatments *in vivo* in ErbB2-driven xenograft model. All the treatments that were administered are mentioned in Figure 13. Treatments were injected 4 times at 4-day intervals at an equivalent dose of 6 mg-DOX/kg

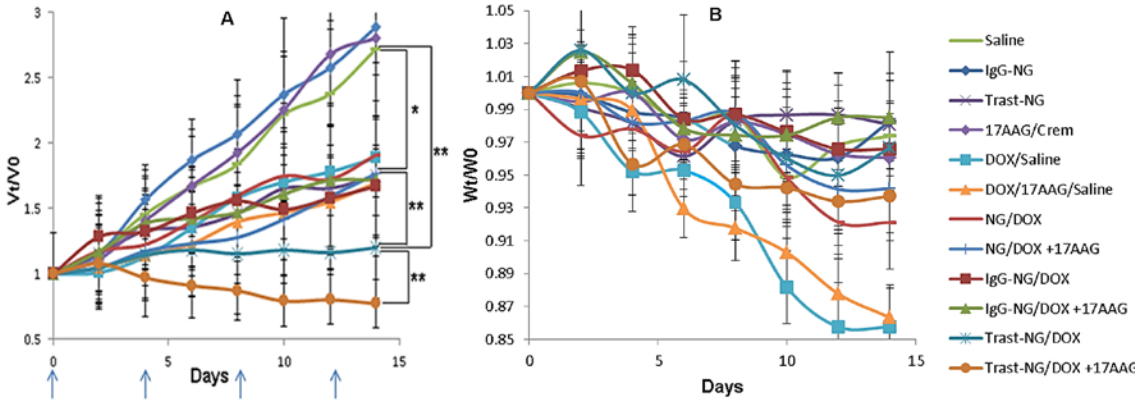

Fig. 13. Relative changes in A) Tumor volume and B) Body weight after administration of ErbB2-targeted Trast-NG/DOX with and without 17AAG co-administration in ErbB2+ - breast cancer mice model. 107 BT-474 cells (an ErbB2 overexpressing human breast cancer cell line) reconstituted in 50% Matrigel were injected directly into the mammary fat pad of 8 week old female Athymic NCr-nu/nu mice. 17-□-Estradiol pellets (0.72mg/pellet; 60 day release) were implanted subcutaneously on the lateral side of the neck of the mice, 3 days prior to the injection of the tumor cells. Values indicated are means ± SEM (n = 10). * p<0.05. ** p<0.01. NG-nanogels, Trast- Trastuzumab, IgG – non-specific human IgG, 17AAG- 17-(allylamino)-17-demethoxygeldanamycin, DOX- doxorubicin.

determined as the maximum tolerated dose upon this treatment schedule. Animals injected with DOX and 17-AAG together received 6mg/kg DOX and 1 mg/kg 17-AAG equivalents per dose (17-AAG was administered 2 hours post DOX or nanogel injections). The changes in the relative tumor volume and body weight are shown in Fig. 13A and 13B, respectively. Tumor burden was significantly decreased by the treatment with combination of free DOX and 17-AAG (DOX+17-AAG) or NG/DOX (with or without 17 AAG) or IgG-NG/DOX (with or without 17 AAG) (P<0.05) treatments compared to control (Fig. 13A). Notably, treatment with 17-AAG alone did not have any substantial effect on the tumor growth and only minor increase in survival was observed over controls (Saline

and IgG/NG) (Fig. 14). In contrast, nearly complete inhibition of tumor growth was observed for the mice treated with Trast-NG/DOX from day 0 to 14, and this effect was potentiated when it was co-administered with 17-AAG, which led to the shrinkage of the tumors ($P < 0.01$) (Fig. 13A). This better effect in tumor reduction translated into increased overall survival of the animals treated with Trast-NG/DOX or Trast-NG/DOX co-administered with 17-AAG compared to any other treatment regimen (Fig. 14). Figure 13B shows that drug-loaded nanogels did not induce body weight loss compared to control while the same dose of the free DOX+17-AAG produced a considerable body weight loss ($P < 0.05$), which indicated systemic toxicity of free drugs.

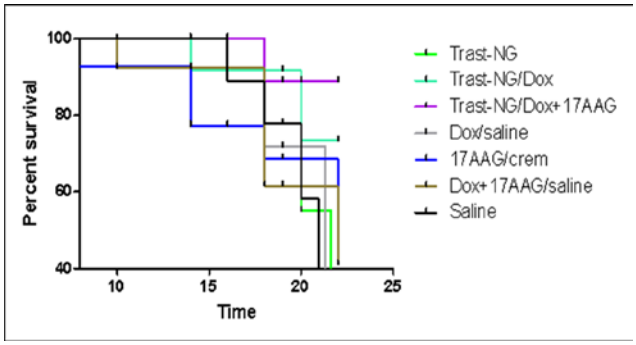

Fig. 14. Kaplan–Meier analysis of overall survival of the animals treated by Trast-NG/DOX with and without 17AAG co-administration in ErbB2+ - breast cancer mice model.

Motivated with our preliminary *in vivo* animal data, we decided to pursue another round of animal experiments with only selected groups to elucidate the various underlying mechanisms of tumor reduction and to follow the total survival of the animals.

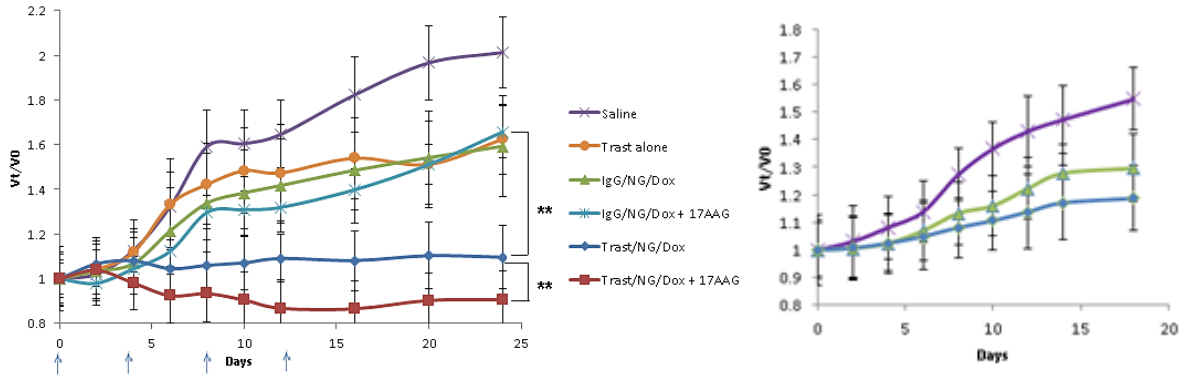

Fig. 15. Relative changes in Tumor volume after administration of ErbB2-targeted Trast-NG/DOX with and without 17AAG co-administration in (**A**) ErbB2+ and (**B**) ErbB2 - breast cancer mice model.

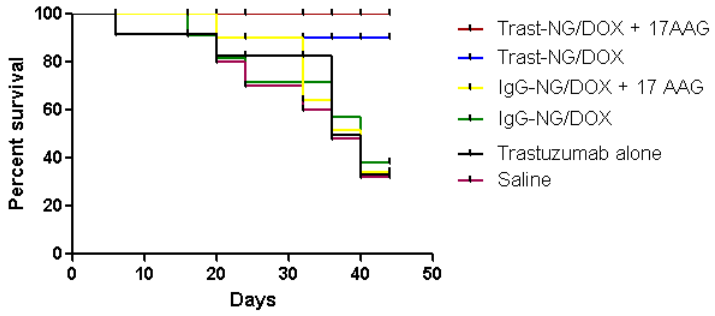

Fig. 16. Kaplan–Meier analysis of overall survival of the animals treated by Trast-NG/DOX with and without 17AAG co-administration in ErbB2+ - breast cancer mice model.

As shown in Figure 15A and 16, antitumor data obtained was in well agreement with our previous studies. As expected, no significant difference of Trastuzumab conjugation was noted in similar experiments conducted on the ErbB2-low MCF-7 tumors (Fig. 15B). These findings support hypothesis that HSP90-inhibition can indeed lead to enhancement of targeted delivery of Doxorubicin specifically into ErbB2+ breast cancer cells (and not in ErbB2- breast cancer cells).

Supplementary studies towards manuscript and future grant applications

Evaluate the synergistic cytotoxicity of the (DOX+17-AAG)-loaded biodegradable nanogel in ErbB2+ breast cancer mouse model: The cytotoxic effects of the DOX and 17-AAG combination have been reported in literature. We have previously demonstrated that the cytotoxic efficacy of 17-AAG plus DOX combination against ErbB2-overexpressing breast cancer cell lines was retained when they were co-encapsulated in biodegradable PEG-polypeptide-based nanogel formulation. Motivated by the enhanced *in vitro* efficacy of (DOX+17-AAG)/NG formulation, we evaluated its antitumor efficacy *in vivo* in ErbB2-driven xenograft model. Free DOX and DOX/NG were injected 4 times at 4-day intervals at an equivalent dose of 6 mg-DOX/kg determined as the maximum tolerated dose upon this treatment schedule. Animals injected with (DOX+17-AAG)/NG received 6mg/kg DOX and 1 mg/kg 17-AAG equivalents per dose. The changes in the relative tumor volume, body weight and animal lifespan are shown in Fig. 17A, 17B and 17C respectively. Tumor burden was significantly decreased by treatments with combination of free drugs (DOX+17-AAG) or DOX-loaded nanogels (DOX/NG) compared to control (P<0.05, Fig. 17A). However, survival of the animals treated with DOX/NG was higher than in animals treated with free DOX+17-AAG between days 0 and 22 which could be due to the systemic toxicity observed upon the treatment with combination of free drugs, DOX+17-AAG (Fig. 17C). Notably, treatment with 17-AAG/NG did not have any substantial effect on the tumor growth and only minor increase in survival was observed over controls (Fig. 17A and 17C). In contrast, nearly complete inhibition of tumor growth was observed for the mice treated with

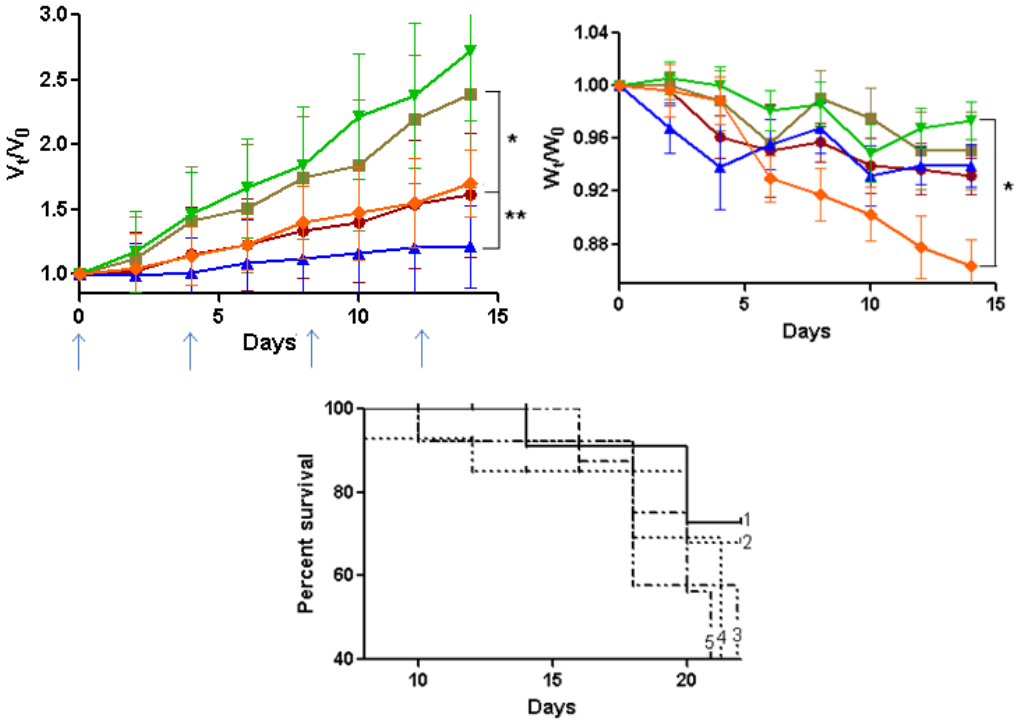

Fig. 17. *In vivo antitumor efficacy of (Dox + 17-AAG)/NG in in ErbB2+ - breast cancer mice model* – Nu/Nu mice carrying xenografts of the ErbB2-overexpressing cell line, BT-474, were treated with free drugs or NG-formulations as described in the methods section. Relative changes in (A) tumor volume and (B) body weight were measured following intravenous administration of (Dox + 17-AAG)/NG (▲) or Dox/NG (●) or Dox + 17-AAG (♦) or 17-AAG/NG (■) or 5% dextrose (▼). Drug formulations were injected in 100 µL at a dose of 6 mg Dox or 1mg 17-AAG equivalents/kg body weight 4 times at 4-day intervals as indicated by the arrows. Values indicated are means ± SEM (n = 10). (C) Kaplan–Meier analysis of overall survival in (Dox + 17-AAG)/*cl*-micelles group (1) or Dox/NG group (2) or Dox + 17-AAG group (3) or 17-AAG/NG group (4) or control group (5). Tumor volume and body weight are normalized with respect to tumor volume or body weight at day 0. * P<0.05, ** P<0.01.

(DOX+17-AAG)/NG from day 0 to 14, which translated into increased overall survival of the animals treated with (DOX+17-AAG)/NG compared to either free DOX+17-AAG or DOX/NG (P<0.05, Fig. 17A & 17C). To further corroborate the superior antitumor efficacy of binary drug combination in nanogels, the tumors were excised post-treatment (on 10th day after last injection) and processed for staining of Ki-67 to examine the effect of treatment on cell proliferation. The number of Ki-67 positive cells were significantly lower in tumors from mice that received (DOX+17-AAG)/NG compared to tumors in control *(P*<0.001*)* or DOX+17-AAG *(P*<0.01*)* or DOX/NG *(P*<0.05*)* (Fig. 18A). Figure 17B shows that either single or binary drug-loaded nanogels did not induce body weight loss compared to control while the same dose of the free DOX+17-AAG produced a considerable body weight loss (P < 0.05), which indicated systemic toxicity of free drugs. Light microscopic examination of H&E stained tissue (liver, spleen, heart kidney and lung) sections from sacrificed animals (day 22) did not show any evidence of toxicity (data not shown). Collectively, these results demonstrate that biodegradable PEG-polypeptide-based nanogels carrying DOX and 17-AAG drug combination exerted superior antitumor efficacy, both in terms of tumor inhibition and survival, which could be attributed to the preferential simultaneous accumulation, and increased potency.

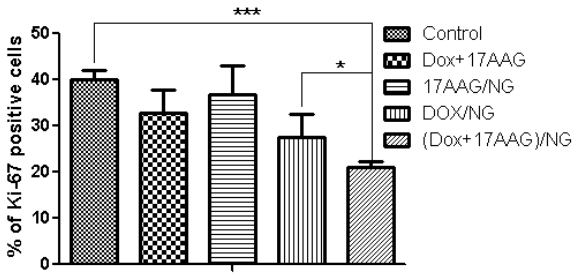

Fig 18. *Ki-67-positive cell proliferation assay of excised tumors from mice treated with free drugs or NG-formulations. * P*<0.05, *** *P*<0.001.

Key Research Accomplishments:

1. We developed a robust and versatile synthetic approach for fabrication of nanogels of core-shell morphology based on block copolymers.

2. A representative panel of nanogels was synthesized using poly(ethylene glycol)-*b*-poly(methacrylic acid) block copolymers of different structure and compositions.

3. The chemical structure of the block copolymer is a key parameter determining the formation of templates for the nanofabrication of nanogels.

4. The physicochemical characteristics of the nanogels (dimensions, swelling behavior) can be tuned by changing the cross-linking density of the cores of the nanogels or by using cross-linkers with different chemical structures. The incorporation of more hydrophobic cross-linkers into the core of the nanogels resulted in the formation of nanogels with smaller sizes and with higher density of cross-links.

4. Doxorubicin, a model chemotherapeutic drug, can be loaded into cross-linked cores of the nanogels with high loading capacity (up to 42 w/w%).

5. The nanogels containing drug combinations (Doxorubicin and 17-AAG) were prepared and characterized.

6. Biodistribution studies on non-targeted Doxorubicin-nanogels demonstrated thatthe nanogels showed an efficient systemic delivery of the drug to human tumor xenografts.

7. A reproducible and robust methodology to conjugate anti-ErbB2 therapeutic antibody Trastuzumab to nanogels was established.
8. Trastuzumab-conjugated nanogels were demonstrated to selectively bind to ErbB2+ tumor cells at high levels compared to untargeted nanogels.
9. Low concentrations of 17AAG were shown to facilitate nanogels endocytosis into lysosomes and deliver DOX inside the tumor cell.
10. Trastuzumab-conjugated nanogels in combination with 17AAG selectively inhibited proliferation and induced apoptosis in ErbB2+ breast cancer cell lines.
11. In a xenograft model, Trastuzumab-conjugated and DOX-loaded nanogels exhibited significantly enhanced efficacy selectively against ErbB2+, indicating that active targeting facilitates tumor specific drug delivery.
12. Concurrent administration of a low, non-toxic, dose of 17AAG substantially enhanced the efficacy of DOX-loaded and Trastuzumab-conjugated nanogels and led to xenograft tumor regression.
13. Importantly, the animals treated with nanogel-encapsulated DOX showed significantly lower systemic toxicity compared to the free drug.

Reportable Outcomes:

Overall Summary of Achievements:

Invited Presentations

1. "Engineering of Soft Nanomaterials for Drug Delivery: Opportunities and Challenges"" University of North Carolina at Chapel Hill, Chapel Hill, NC, July, 2011
2. "Ionic Nanogels as a Versatile Platform for Drug Delivery in Tumor", 2nd International Summer School "Nanomaterials and Nanotechnologies in Living Systems", Moscow Region, Russia, September, 2011.
3. "Ionic nanogels for drug delivery in cancer". NanoDDS'12; Atlantic City, New Jersey; Dec 6 2012.
4. " Dysregulated Endocytosis in Cancer". NIH NCI Workshop January 10-11, 2013.

Conference Presentations

1. "Mechanism-based enhancement of ErbB2-targeted delivery of chemotherapeutics encapsulated in Trastuzumab-conjugated polymeric nanocarriers". Srikumar M. Raja, Jong Oh Kim, Swapnil S. Desale, Natasha V. Nukolova, Hardeep S. Oberoi, Stetson H. Williams, Haitao Luan, Vimla Band, Alexander V.Kabanov, Tatiana K. Bronich, Hamid Band. *American Association of Cancer Research,* 102nd Annual meeting, Chicago, Il, March 31-April 4, 2012.
2. "Mechanism-based enhancement of ErbB2-targeted delivery of chemotherapeutics encapsulated in Trastuzumab-conjugated polymeric nanocarriers". Swapnil Desale, Srikumar M. Raja**,** Jong Oh Kim, Stetson H. Williams, Haitao Luan, Vimla Band, Tatiana K. Bronich, Hamid Band. *Gordon Research Conference.* Vermont, July14-19, 2013.

Manuscripts under preparation:

1. Swapnil S. Desale*, Srikumar M. Raja*#, Jong Oh Kim, Bhopal Mohapatra, Kruti S. Soni, Samuel M. Cohen, Haitao Luan, Dan Feng, Timothy Bielecki, Matthew Stork,

Stetson H. Williams, Vimla Band, Hamid Band#, and Tatiana K. Bronich# (2014). Mechanism-based enhancement of ErbB2-targeted delivery of chemotherapeutics encapsulated in Trastuzumab-conjugated polymeric nanocarriers (*Equal Contribution; #Co-Corresponding Authors).

2. Srikumar M. Raja*#, Swapnil S. Desale*, Jong Oh Kim, Bhopal Mohapatra, Kruti S. Soni, Samuel M. Cohen, Haitao Luan, Stetson H. Williams, Matthew Storck, Vimla Band, Hamid Band#, and Tatiana K. Bronich#. (2014). Polypeptide-based nanogels co-encapsulating synergistic combination of Doxorubicin with 17-AAG show potent anti-tumor activity in ErbB2-driven breast cancer models (*Equal Authors; #Co-Corresponding Authors).
3. Raja, S.M.#, Bronich, T.K.#, Swapnil S. Desale, Band, V. and Band, H.# (2014) ErbB-receptor endocytic pathway and targeted nanoparticulate drug-delivery systems in Breast Cancer treatment. (Review article) (Co-Corresponding Authors)

Conclusions:

In conclusion, we have successfully accomplished all of the goals of BC102673 award with dramatic positive outcomes. The proof of concept provided by these studies have established and validated a new, mechanism-based targeted therapy platform against ErbB2+ breast cancers. Our approach is fundamentally paradigm-shifting by allowing high concentrations of toxic drugs to be encapsulated in targeted nanogels but concurrently enhancing their entry into target cells using 17AAG as a facilitator of ErbB2-mediated nanogel endocytosis into lysosomes.

The novel concept established here together with technical achievements to prepare scalable batches of nanogels with anti-ErbB2 antibody as a targeting moiety and high concentrations of anticancer drugs encapsulated in the core have opened a clear translational avenue to move the nanogels developed here towards clinical use in breast cancer treatment.

References:

1. Hommelgaard AM, Lerdrup M, van Deurs B. Association with membrane protrusions makes ErbB2 an internalization-resistant receptor. Mol Biol Cell 2004;15(4):1557-67.
2. Lerdrup M, Hommelgaard AM, Grandal M, van Deurs B. Geldanamycin stimulates internalization of ErbB2 in a proteasome-dependent way. J Cell Sci 2006;119(Pt 1):85-95.
3. Lerdrup M, Bruun S, Grandal MV, et al. Endocytic down-regulation of ErbB2 is stimulated by cleavage of its C-terminus. Mol Biol Cell 2007;18(9):3656-66.
4. S. Bontha, A.V. Kabanov, T.K. Bronich, Polymer micelles with cross-linked ionic cores for delivery of anticancer drugs, *J. Control. Release* 2006, 114, 163–174
5. T.K. Bronich, P.A. Keifer, L.S. Shlyakhtenko, A.V. Kabanov, Polymer micelle with cross-linked ionic core, *J. Am. Chem. Soc.* 2005, 127, 8236–8237.
6. J.O. Kim, N.V. Nukolova, H.S. Oberoi, A.V. Kabanov, T.K. Bronich, Block ionomer complex micelles with cross-linked cores for drug delivery, *Polymer Science Series A* 2009, 51, 708-718.
7. Raja SM, Clubb RJ, Bhattacharyya M, et al. A combination of trastuzumab and 17-AAG induces enhanced ubiquitinylation and lysosomal pathway-dependent ErbB2 degradation and cytotoxicity in ErbB2- overexpressing breast cancer cells. Cancer Biol Ther 2008;7(10):1630-40.
8. Waterhouse, D.N., Tardi, P. G., Mayer, L. D., Bally, M. B., A comparison of liposomal formulations of doxorubicin with drug administered in free form: changing toxicity profiles. *Drug Saf*, 2001. 24, 903-20.
9. Patil, R.R., Guhagarkar, S.A., Devarajan, P.V., Engineered Nanocarriers of Doxorubicin: A Current Update. *Crit Rev Ther Drug Carrier Syst,* 2008, 25, 1-61.
10. Lu, W.-L., Qi, X-R., Zhang, Q., Li, R-Y., Wang, G-L., Zhang, R-J., A Pegylated Liposomal Platform: Pharmacokinetics, Pharmacodynamics, and Toxicity in Mice Using Doxorubicin as a Model Drug. *J Pharmacol Sci*, 2004, 95, 381-389.
11. Allen, T.M., Hansen, C.B., de Menezes, D.L, Pharmacokinetics of long-circulating liposomes *Adv Drug Delivery Rev*, 1995, 16, 267-284.